

## Multi-frequency VLBI studies of the optically violent variable quasar NRAO 530

---

R.-S. Lu<sup>\*1,2</sup>, T. P. Krichbaum<sup>1</sup>, & J. A. Zensus<sup>1</sup>

1. Max-Planck-Institute für Radioastronomie, Germany

2. Shanghai Astronomical Observatory, Chinese Academy of Sciences

E-mail: rslu, tkrichbaum, azensus@mpifr-bonn.mpg.de

NRAO 530 (also known as 1730-130) is being studied by high-frequency VLBI observations. We investigate the frequency-dependent position shifts of jet components, and the detailed jet kinematics over the last ten years. We find significant position shifts for 3 jet components (component *d*, *e*, and *f*) with a mean shift of  $-0.15 \pm 0.02$  mas between 22 and 43 GHz and detected for the first time a 2-dimensional position shift (component *f*) indicative of oblique structures. We obtained apparent velocities of 8 jet components with  $\beta_{\text{app}}$  ranging from  $(2-26)c$ . Accordingly, we estimated jet physical parameters with a minimum Lorentz factor of 14 and Doppler factors in the range of 14 and 28 (component *f*). The observed variations in the morphology of NRAO 530 are related to the motion of separate jet components along the jet, with the most pronounced changes occurring near the core. We estimated a position angle swing of  $4^\circ$  per year for jet component *d*. The non-ballistic motion and change of jet orientation makes this source another prominent example of a helical and possibly “swinging/wobbling” jet, such as BL Lac or NRAO 150.

*10th European VLBI Network Symposium and EVN Users Meeting: VLBI and the new generation of radio arrays*

*September 20-24, 2010*

*Manchester, UK*

---

\*Speaker.

## 1. Introduction

NRAO 530 is an optically violent variable blazar at a redshift of  $z = 0.902$  [1]. Violent broadband variability has been observed in the radio [2], optical [3], and through to the  $\gamma$ -ray regime [4]. In  $\gamma$ -rays, it was relatively quiescent after the launch of Fermi [5], but at present is flaring again [6]. NRAO 530 exhibits two-sided lobes in the east-west direction on kpc scales [7]. Centimeter VLBI maps showed a core-jet structure on pc scales with an oscillating trajectory extending to the north from the core [8]. Space VLBI observations revealed brightness temperatures of NRAO 530 significantly in excess of both, the inverse Compton and the equipartition limit [9]. Superluminal motions of several components were detected with  $\beta_{\text{app}}$  in the range of  $10\text{--}40c$  [2, 7, 10].

Throughout this manuscript, we adopt the luminosity distance to NRAO 530  $D_L = 5.8$  Gpc, 1 mas of angular separation corresponding to 7.8 pc, and a proper motion of  $1 \text{ mas yr}^{-1}$  corresponding to a speed of  $\beta_{\text{app}} = 48.5c$  ( $H_0 = 71 \text{ km s}^{-1} \text{ Mpc}^{-1}$ ,  $\Omega_M = 0.27$ ,  $\Omega_\Lambda = 0.73$ ).

## 2. Observations and data reduction

During a global campaign on Sgr A\* in May 2007, NRAO 530 was monitored as a calibrator and fringe tracker with the VLBA from 15 to 24 May 2007 (2007.370–2007.395) at 22, 43, and 86 GHz on 10 consecutive days [11]. NRAO 530 was observed shortly before, during, and after the time of visibility of Sgr A\*. The data reduction was performed within the AIPS software in the usual manner. In order to probe the jet kinematics and to increase the time coverage, we have also added VLBA observations at 15 GHz from the 2 cm survey and MOJAVE program observed between 1999 and 2009, spanning altogether 10 years<sup>1</sup>. These data were provided as automatically self-calibrated *uv* FITS file, which we re-calibrated and re-mapped in *difmap* before model-fitting.

## 3. Results and discussion

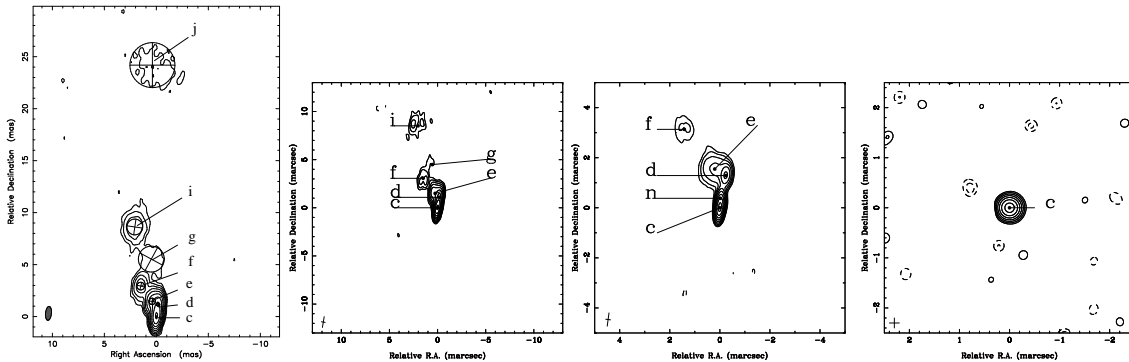


**Figure 1:** Clean maps of NRAO 530 at 15, 22, 43, and 86 GHz (from left to right). Image parameters are given in Table 1.

In Fig. 1, we show some CLEAN maps at 15, 22, 43, and 86 GHz as examples. Table 1 lists the map parameters. On VLBI scales, NRAO 530 is characterized by a one-sided jet following a curved

<sup>1</sup>This research has made use of data from the MOJAVE database that is maintained by the MOJAVE team (Lister et al., 2009, AJ, 137, 3718)

**Table 1:** Description of VLBA images of NRAO 530 shown in Fig. 1.

Epoch	$\nu$	$S_{\text{peak}}$	Restoring Beam			Contours
			Major	Minor	P.A.	
	GHz	Jy/beam	mas	mas	deg	
(1)	(2)	(3)	(4)	(5)	(6)	(7)
2007.441	15	1.20	1.34	0.568	-5.7	-0.35, 0.35, 0.7, ..., 89.6
2007.370	22	1.32	1.19	0.344	-12.8	-0.3, 0.3, 0.6, ..., 76.8
2007.370	43	1.33	0.537	0.193	-7.7	-0.3, 0.3, 0.6, ..., 76.8
2007.370	86	0.74	0.2	0.2	0	-1, 1, 2, ..., 64

trajectory extending up to  $\sim 25$  mas north of the core. As can be seen in Fig. 1, our data reveal a jet morphology with richer structure seen at lower frequencies. The inner jet extends slightly to the north-west direction (P.A.  $\sim -10^\circ$ ) out to a core separation of  $\sim 1.5$  mas and then bends sharply by  $\sim 90^\circ$  towards a P.A.  $\sim 25^\circ$  at a core separation of 3.5 mas. From there, the jet bends gently northward following a curved path with underlying diffuse emission. Finally, it fades away at a core separation of  $\sim 9$  mas with a P.A. of  $10^\circ$ . The jet component (*i*) located at  $\sim 25$  mas north of the core is not seen at the three highest frequencies. However, it is visible at 15 GHz across all the epochs, likely due to its steep spectrum and higher brightness at 15 GHz.

### 3.1 Frequency-dependence of component positions

The measurements at 22, 43, and 86 GHz repeated every day for 10 days, allow us to investigate the frequency-dependent position shift of the jet components. In Fig. 2 we plot the core separation against position angle for the jet components detected at least at two of these three frequencies, along with the spectra of the core and components *d*, *e*, and *f*. The relative positions of three components (*d*, *e*, and *f*) are shifted systematically between 22 and 43 GHz. For all three components, the core separation at 43 GHz is significantly ( $> 3\sigma$ ) larger than that at 22 GHz. The shift between 22 and 43 GHz is  $-0.17$ ,  $-0.12$ , and  $-0.14$  mas, respectively, with a mean of  $-0.15 \pm 0.02$  mas. For the P.A., however, only component *f* shows significant displacements (at the  $> 4\sigma$  level). The measured position of component *d* at 86 GHz is consistent with that at lower frequencies, in the sense that the core distance at 86 GHz is larger than that at lower frequencies. For component *n*, we are unable to compare the position shift between 43 and 86 GHz limited mainly by the large position scatter at 86 GHz. In addition, the 15 GHz data also provide consistency checks for the components *d*, *e*, and *f*.

A well known effect which causes the frequency dependence of jet component position is the so called ‘‘core shift’’ [13]). The location of the self-absorbed VLBI core depends on the  $\tau = 1$  surface. It depends on the observing frequency and the distance to the central engine,  $r_{\text{core}} \propto \nu^{-1/k_r}$ , where  $k_r$  is related to the electron energy distribution, the magnetic field, and the particle number density. For a self-absorbed core, which is in energy equipartition between particles and magnetic fields, one can show that  $k_r = 1$  [13]. Since the absolute position information for VLBI observations is lost due to phase self-calibration, position shifts are normally measured by referencing the core to some optically thin jet components. For the latter their positions are expected to be frequency-independent. Fig. 2 also indicates that the displacement of component positions are not all in the

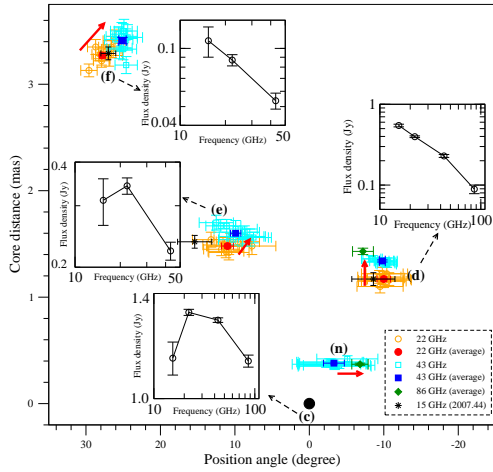


**Figure 2:** Core separation plotted against position angle for the inner jet components. Different symbols denote different frequencies with filled symbols representing the average position at 22 (filled circles), 43 (filled squares) and 86 GHz (filled diamonds). To prevent confusion, only mean values are shown at 86 GHz. A clear frequency-dependent displacement of the jet component positions is seen and is indicated by red arrows. Spectra are shown for those components visible at more than 2 frequencies (insets).

same direction. In other words, we observe non-radial shifts, which may indicate two dimensional gradients of the jet parameters (magnetic field, particle number density, opacity), an effect which is expected if a bent jet is observed at small viewing angles.

### 3.2 Jet kinematics at 15 GHz

The plot of the core separation of the jet components against time, is shown in Fig. 3. It facilitated the component cross-identification across the epochs. To measure the separation speeds of the individual features, we applied a linear regression analysis to the data. The fit results are shown in Fig. 3 as dashed lines with apparent speeds in the range of (2–26)  $c$ .

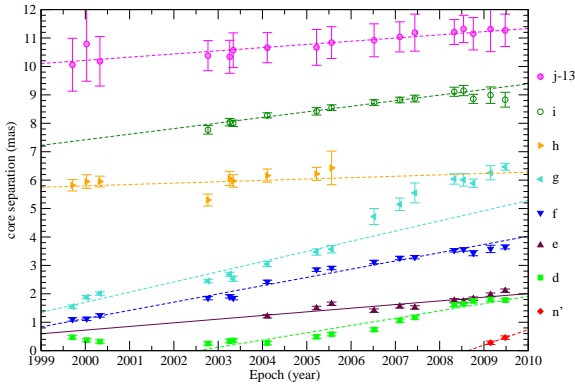


**Figure 3:** Separation from the core as a function of time for the inner jet components in NRAO 530. The core separations of component  $j$  has been shifted by 13 mas downwards for display purposes. The dashed lines are linear regression fits to the data.

Component  $n'$  was ejected around 2008.6, which coincides with a moderate flux density flare seen in late 2008 at millimeter wavelengths<sup>2</sup> and in early 2009 at centimeter wavelengths [14]. The identification of the component  $d$  at epochs before 2001 is subject to uncertainties due to time gaps in the data. So is the relation between its ejection and the moderate flare around 2002 [7]. Component  $f$  and  $g$  can be identified with components B and E seen by [10]. The derived apparent speeds (14  $c$  and 21  $c$ ) are slightly faster than their findings (10  $c$  and 14  $c$ ), likely due to a

<sup>2</sup>cf. <http://sma1.sma.hawaii.edu/callist/callist.html?data=1733-130>

shorter time coverage ( $\sim 4$  yr). The ejection time of both components is in the range of a dramatic outburst/activity phase occurring between 1994 and 1998. However, due to the expansion effects, the uncertainty in the position measurement for component *g* becomes systematically larger at later epochs. We note that component *g* also shows strong evidence for acceleration. The linear fit to its motion is only a rough approximation. Component *e* and the three outer components (*h*, *i*, and *j*) reveal relatively slow motions with  $\beta_{\text{app}}$  in the range of  $2-9c$ .

The measured apparent velocities can be used to estimate the parameters of the jet, using the superluminal motion equation,  $\beta_{\text{app}} = \frac{\beta \sin \theta}{1 - \beta \cos \theta}$ , where  $\beta_{\text{app}}$  and  $\beta$  are the apparent and the true velocity in units of the speed of light  $c$  and  $\theta$  is the angle between the direction of motion and the line of sight. Adopting the apparent speed of component *f* ( $\beta_{\text{app}} = 14.1c$ ), which is the fastest component with a reliable velocity measurement, we derive a lower limit on the Lorentz factor  $\Gamma$ ,  $\Gamma_{\text{min}} = \sqrt{1 + \beta_{\text{app}}^2} = 14.1$ . For the maximum allowable viewing angle  $\theta_{\text{max}}$  we obtain  $8.1^\circ$ . The critical viewing angle, which maximizes  $\beta_{\text{app}}$  for given  $\beta$ , is  $\theta_{\text{cri}} = \arcsin(\frac{1}{\Gamma})$ . For component *f*, we find  $\theta_{\text{cri}}$  is  $4.1^\circ$ . Correspondingly, we can also derive a Doppler factor  $\delta_{\text{min}}$  using the minimum Lorentz factor  $\Gamma_{\text{min}}$  and  $\theta_{\text{cri}}$ . For component *f*,  $\delta_{\text{min}}$  is 14.1. For even smaller angles ( $\theta \rightarrow 0$ ),  $\delta$  tends to the limit of  $\sim 2\Gamma = 28.2$ .

### 3.3 Morphology and its evolution

A comparison of the projected trajectories of the jet components in 1997 [10] and 2007 indicates that the morphology of the jet changed significantly. Obviously, the major differences appear in the regions close to the core, in contrast to the relative stability of the outer jet. This can be attributed to the relatively fast motion of the inner jet components. Fig. 4 (left) shows the evolution of the jet ridge line over the last 10 years obtained using the 15 GHz data. This plot illustrates that the morphology of the jet changes from epoch to epoch due to the non-ballistic motion of the jet components. Shown in Fig. 4 (right) is the evolution of the inner jet axis with the component *d* being the tracer. Both radial and non-radial motion is observed for this component. Most notably a jet position angle swing of  $\sim 4^\circ/\text{yr}$  can be estimated (between 1999 and 2009).

Using mm-VLBI data, [15] reported a jet position angle swing of  $\sim 11^\circ/\text{yr}$  associated with non-ballistic superluminal motion in NRAO 150. It is not clear whether the swing speed increases for jet components even closer to the core of NRAO 530. However, the data at 15 GHz do not allow us to investigate the evolution of the innermost jet components, like e.g. for component *n*. Therefore, future VLBI monitoring observations at higher frequencies are needed to further study this effect.

## 4. Summary

We studied the pc-scale jet properties of NRAO 530 with high-resolution multi-epoch VLBI observations. For 3 components, we find significant position shifts between 22 and 43 GHz, which can be interpreted as the result of a core shift effect. One component (*f*) shows a two-dimensional position shift. This indicates that the variations of the optical depth, which induces the core-shift, have also a non-radial dependence (e.g. caused by an oblique shock). We measured a superluminal motion for 8 components with apparent speeds  $\beta_{\text{app}}$  in the range of  $2-26c$ . For the fastest com-

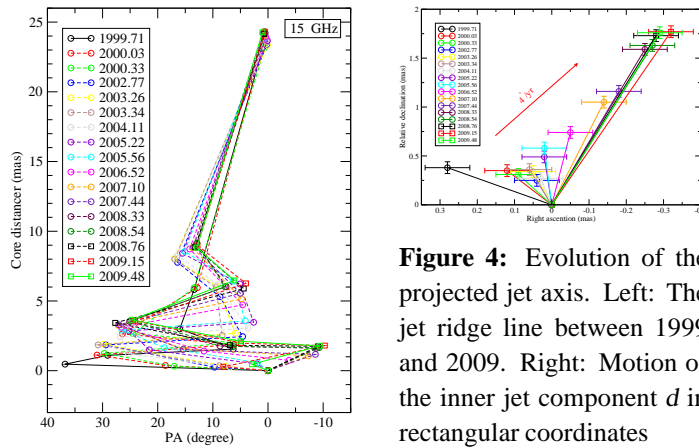


**Figure 4:** Evolution of the projected jet axis. Left: The jet ridge line between 1999 and 2009. Right: Motion of the inner jet component  $d$  in rectangular coordinates

ponent, we obtained a minimum Lorentz factor of 14 and Doppler factors in the range of 14 and 28.

The morphology of NRAO 530 has varied significantly over the past 10 years (between 1997 and 2007). The variations are more pronounced near the core. Moreover, we found significant variations of the jet position angle and no common trajectory for the jet components. For component  $d$ , we estimated a swing of  $\sim 4^\circ$  per year between 1999 and 2009. The observed non-ballistic motion and a pronounced change of the jet orientation makes NRAO 530 another prominent example of a “swinging/wobbling” jet, similar to e.g. NRAO 150 [15].

## References

- [1] Junkkarinen, V. 1984, *PASP*, 96, 539
- [2] Bower, G. C., Backer, D. C., Wright, M., et al. 1997, *ApJ*, 484, 118
- [3] Webb, J. R., Smith, A. G., Leacock, R. J., et al. 1988, *AJ*, 95, 374
- [4] Mukherjee, R., et al. 1997, *ApJ*, 490, 116
- [5] Abdo, A. A., et al. 2009, *ApJ*, 700, 597
- [6] D’Ammando, F, Vandenbroucke, J. *ATel*, 3002
- [7] Hong, X.-Y., Sun, C.-H., Zhao, J.-H., et al. 2008, *ChJAA*, 8, 179
- [8] Shen, Z.-Q., et al. 1997, *AJ*, 114, 1999
- [9] Bower, G. C., & Backer, D. C. 1998, *ApJL*, 507, L117
- [10] Feng, S.-W., Shen, Z.-Q., Cai, H.-B., Chen, X., Lu, R.-S., & Huang, L. 2006, *A&A*, 456, 97
- [11] Lu, R.-S., Krichbaum, T. P., Eckart, A., et al. 2010, *A&A*, in press
- [12] Chen, Y. J., Shen, Z.-Q., & Feng, S.-W. 2010, *MNRAS*, 408, 841
- [13] Lobanov, A. P. 1998, *A&A*, 330, 79
- [14] Aller, M. F., Aller, H. D., & Hughes, P. A. 2009, arXiv:0912.3176
- [15] Agudo, I., et al. 2007, *A&A*, 476, L17 1994, *A&A*, 284, 51 Witzel, A., & Karouzos, M. 2008, *A&A*, 483, 125